$CuAg(SO_4)_2$: A doubly strongly correlated altermagnetic three-dimensional analog of the parent compounds of high-T_c cuprates – Supplemental Material –

Harald O. Jeschke,[1] Makoto Shimizu,[2] and Igor I. Mazin[3]

[1] *Research Institute for Interdisciplinary Science, Okayama University, Okayama 700-8530, Japan*
[2] *Department of Physics, Graduate School of Science, Kyoto University, Kyoto 606-8502, Japan*
[3] *Department of Physics and Astronomy, and Quantum Science and Engineering Center, George Mason University, Fairfax, Virginia 22030, USA*

(Dated: June 24, 2024)

Additional DFT results

In Fig. S1, we identify the character of the bands of $CuAg(SO_4)_2$ near the Fermi level by showing the Ag $4d$ and Cu $3d$ orbital weights, respectively. The local coordinate system is appropriately chosen with x and y pointing towards nearest Ag-O or Cu-O bonds and z pointing towards the apex of the elongated octahedra. The orbital character of the four bands at the Fermi level is dominated by Ag $4d_{x^2-y^2}$ and Cu $3d_{x^2-y^2}$. Note that

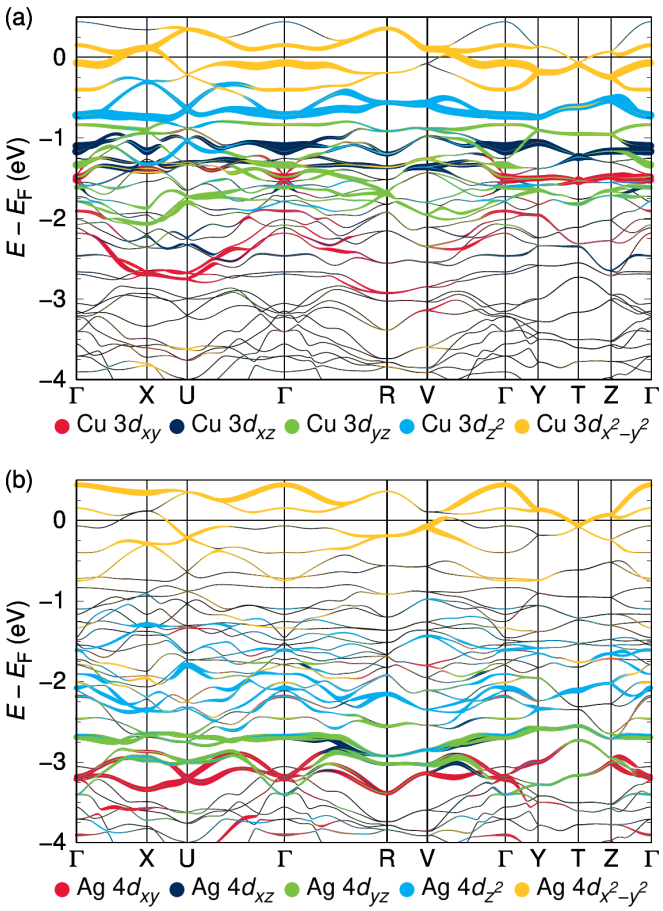

Figure S1. GGA band structure of $CuAg(SO_4)_2$ with (a) orbital weights of Cu and (b) of Ag. Cu $3d$ and Ag $4d$ orbital character, respectively, are highlighted.

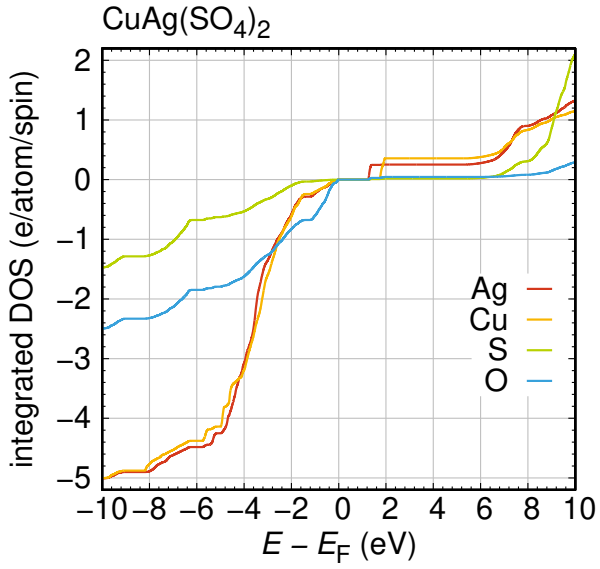

Figure S2. Integrated density of states of $CuAg(SO_4)_2$ at $U_{Ag} = 3.6\,eV$, $U_{Cu} = 4.8\,eV$ in the lowest energy antiferromagnetic state. This corresponds to the density of states shown in Fig. 3 of the main text. The electron count is shown per atom and per spin.

this figure shows nonmagnetic calculations without and DFT+U correction, before the magnetic order shifts different bands into each other. This way it shows more clearly that we have the $d_{x^2-y^2}$ bands near the Fermi level, and the weight is on different bands for Cu and for Ag.

Fig. S2 shows the integrated number of occupied and empty states for $CuAg(SO_4)_2$ in the lowest energy antiferromagnetic $\mathbf{q} = (0, 0, 2\pi)$ state. This is calculated with GGA+U at $U_{Ag} = 3.6\,eV$, $U_{Cu} = 4.8\,eV$ and corresponds to the density of state plot in Fig. 3 of the main text. Note that for total electron numbers, the values have to be multiplied by 2 for spin and by multiplicity in the formula, *i.e.* 2 for S and 8 for O.

In Fig. S3, we demonstrate the spin splitting in the lowest energy AFM state, *i.e.* the property of altermagnetism in $CuAg(SO_4)_2$. Fig. S3 (a) shows the bands along the $\Gamma - R$ path (see Figs. 2 (a) and (b) of the main text for the Ag $4d$ and Cu $3d$ orbital character, respectively). Fig. S3 (b) shows a small energy range, with

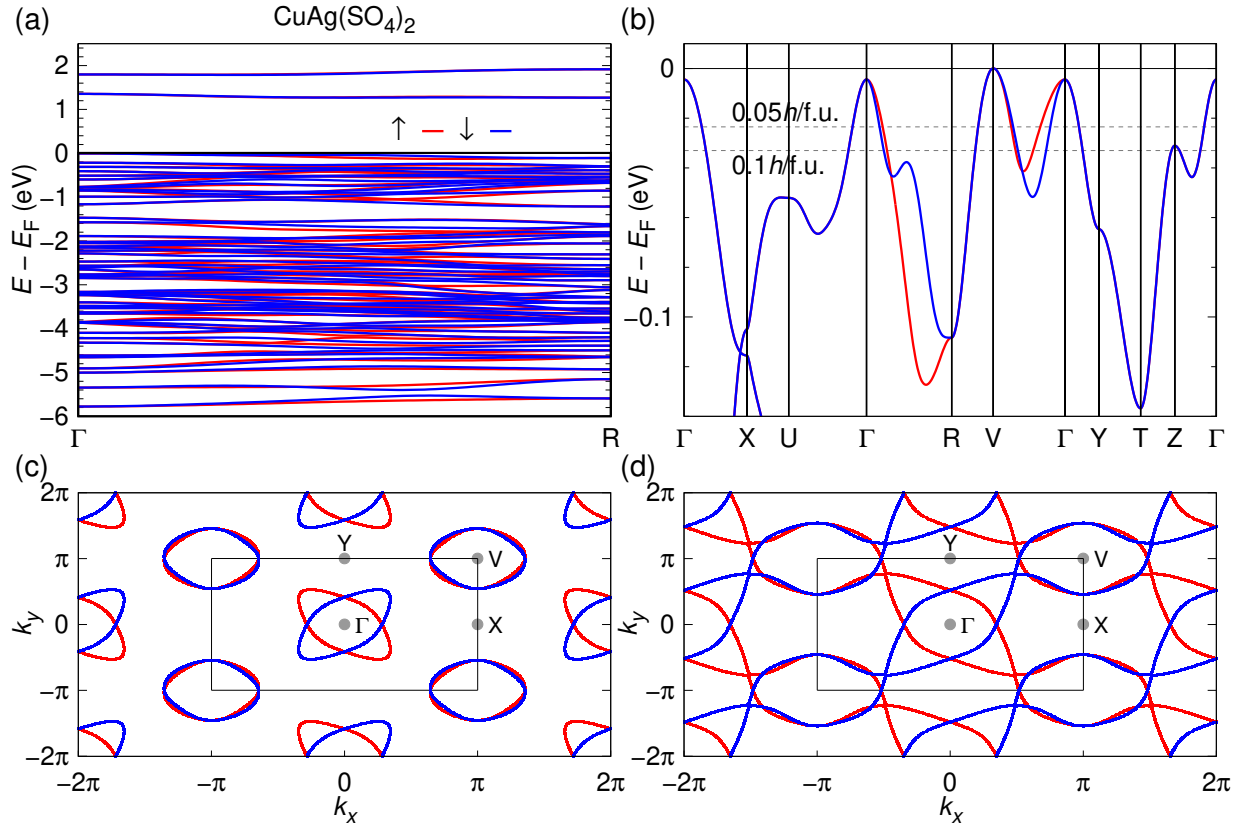

Figure S3. (a) Band structure of $CuAg(SO_4)_2$ in the lowest energy AFM state along the $\Gamma - R$ path, with spin up bands in red and spin down bands in blue. The spin splitting between up and down bands indicates altermagnetism. (b) Small energy range of the full band structure. Energies that correspond to doping with 0.05 and 0.1 holes per formula unit are marked by dashed lines. (c) and (d) Fermi surfaces of $CuAg(SO_4)_2$ in the $k_x - k_y$ plane under hypothetical doping by 0.05 and 0.1 holes per formula unit, respectively.

high symmetry points $X = (1/2, 0, 0)$, $U = (1/2, 0, 1/2)$, $R = (1/2, 1/2, 1/2)$, $V = (1/2, 1/2, 0)$, $Y = (0, 1/2, 0)$, $T = (0, 1/2, 1/2)$, $Z = (0, 0, 1/2)$. Dashed lines mark the energies $E = -23.5\,\text{meV}$ and $E = -33\,\text{meV}$ which would correspond to doping the formual unit with 0.05 and 0.1 holes, respectively. Figs. S3 (c) and (d) show Fermi surfaces under the assumption that doping with 0.05 and 0.1 holes per formula unit could be achieved. In the $k_x - k_y$ plane, these Fermi surfaces which are plotted here in the rigid band approximation would also be spin split due to the altermagnetic nature of $CuAg(SO_4)_2$.

Spin up and spin down sublattices in the $P2_1/n$ space group can be connected by a glide operation, $(x, y, z) \rightarrow (x + \frac{1}{2}, \bar{y} + \frac{1}{2}, z + \frac{1}{2})$. Therefore, the magnetic structure is preserved under a combination of the glide and time reversal operations, which maps

$$\begin{aligned}(k_x, k_y, k_z, \sigma) &\rightarrow (k_x, -k_y, k_z, \sigma) \\ &\rightarrow (-k_x, k_y, -k_z, \bar{\sigma})\end{aligned} \tag{S1}$$

in momentum space [1]. In addition, the magnetic structure is preserved under the inversion operation. Therefore, the magnetic structure is also preserved under the operation, which maps

$$(-k_x, k_y, -k_z, \bar{\sigma}). \rightarrow (k_x, -k_y, k_z, \bar{\sigma}) \tag{S2}$$

in momentum space. Therefore, the electronic state at (k_x, k_y, k_z) of spin up is equivalent to those at $(-k_x, k_y, -k_z)$ and at $(k_x, -k_y, k_z)$ of spin down, and thus

$$\begin{aligned}E_\uparrow(k_x, k_y, k_z) &= E_\downarrow(-k_x, k_y, -k_z) \\ E_\uparrow(k_x, k_y, k_z) &= E_\downarrow(k_x, -k_y, k_z).\end{aligned} \tag{S3}$$

Band splitting in Fig. S3 (b) can be understood with Eq. (S3). The first equation leads to $E_\uparrow(\mathbf{k}) = E_\downarrow(\mathbf{k})$ on $(0, k_y, 0)$, $(0, k_y, \pi)$, $(\pi, k_y, 0)$ and (π, k_y, π) lines, which leads to no band splitting on the k-paths of Γ-Y and T-Z. The second equation leads to $E_\uparrow(\mathbf{k}) = E_\downarrow(\mathbf{k})$ on $k_y = 0, \pi$ planes, which leads no band splitting on the k-path of Γ-X-U-Γ, R-V, Y-T and Z-Γ. Therefore, bands can split on the k-paths of Γ-R and V-Γ.

The Fermi surface cuts in Fig. S3 (c,d) also reflect Eq. (S3). On the $k_z = 0$ plane, the equations become $E_\uparrow(k_x, k_y) = E_\downarrow(-k_x, k_y)$ and $E_\uparrow(k_x, k_y) = E_\downarrow(k_x, -k_y)$. Thus, the Fermi surface of up spin (red) coincides with that of down spin (blue) if it is rotated by 90 degrees around Γ.

Classical molecular field theory

Given the nontrivial exchange Hamiltonian, it is instructive to re-derive the classical molecular field (Weiss) theory specifically for this case. As usual, we introduce the Curie susceptibility $\chi(T) = \mu_{\rm eff}^2/3T$, where $\mu_{\rm eff}^2 = 3$ for $S = 1/2$. Let us assume that in an external field H the two sublattices, Ag and Cu, acquire magnetic moments $M_{\rm A}$ and $M_{\rm C}$. From the previous section, in order of decreasing magnitude, the relevant exchange constants are $J_{\rm AC} = J_4$, $J_{\rm AA} = J_5^{\rm A}$ and $J_{\rm CC} = J_2^{\rm C}$. The molecular field on the site A will be $2M_{\rm C}J_4 + 4M_{\rm A}J_5^{\rm A}$, on C $2M_{\rm A}J_4 + 2M_{\rm C}J_2^{\rm C}$. Thus the Weiss equation will be

$$M_{\rm A} = (H + 2M_{\rm C}J_4 + 4M_{\rm A}J_5^{\rm A})\chi \qquad \text{(S4)}$$

$$M_{\rm C} = (H + 2M_{\rm A}J_4 + 2M_{\rm C}J_2^{\rm C})\chi \qquad \text{(S5)}$$

Solving for M, the Curie-Weiss susceptibility

$$\begin{aligned}\chi_{\rm CW} &= (M_{\rm A} + M_{\rm C})/2H \\ &= \chi\frac{\chi^{-1} - 2J_4 + J_5^{\rm A} + J_2^{\rm C}}{\chi^{-1} + 2J_5^{\rm A} + J_2^{\rm C} + 2\chi(2J_5^{\rm A}J_2^{\rm C} - J_4^2)}\end{aligned} \qquad \text{(S6)}$$

Expanding $1/\chi_{\rm CW}$ in $1/T$, we get the Curie-Weiss law with the same $\mu_{\rm eff} = \sqrt{3}$ and $\theta_{\rm CW} = (2J_4 + 2J_5^{\rm A} + J_2^{\rm C})S(S+1)/3 = (2J_4 + 2J_5^{\rm A} + J_2^{\rm C})/4$, the expression that we used above to fix $U_{\rm eff}$. The reason why Ref. [2] found a surprisingly large $\mu_{\rm eff}^2 = 2.3^2 = 5.3$, corresponding to $S = 0.75$, rather than $S = 1/2$, is unclear at this point.

Comparison to cuprates

In Fig. S4, we show the density of states of the prototypical cuprate superconductor parent compound La_2CuO_4.

Additional DFT energy mapping details

In Table S1, we present the full results of the DFT energy mapping. They were obtained using a 5-fold unit cell of $CuAg(SO_4)_2$ containing ten formula units. This allows resolving all exchange interactions up to twice the nearest neighbor Ag-Cu distance of 3.58 Å. The Hund's rule coupling strength for Cu^{2+} is fixed at $J_{\rm H} = 1\,$eV following previous work [3, 4]. We assume a factor 0.75 between $3d$ and $4d$ interaction values, thus fixing $J_{\rm H} = 0.75\,$eV for Ag^{2+}. The error bars given in brackets reflect the statistical errors of the fit for the energies of 60 distinct spin configurations.

We demonstrate that the DFT energy mapping approach works extremely well in $CuAg(SO_4)_2$ by showing, in Fig. S5, a comparison between DFT energies and energies of the fitted Heisenberg Hamiltonian.

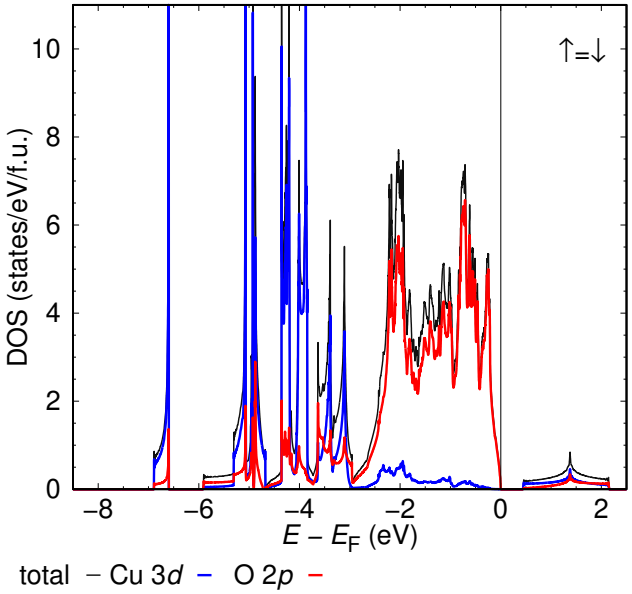

Figure S4. GGA+U density of states of La_2CuO_4 in the Néel state. Spin ↑ and spin ↓ are identical so only spin ↑ is shown.

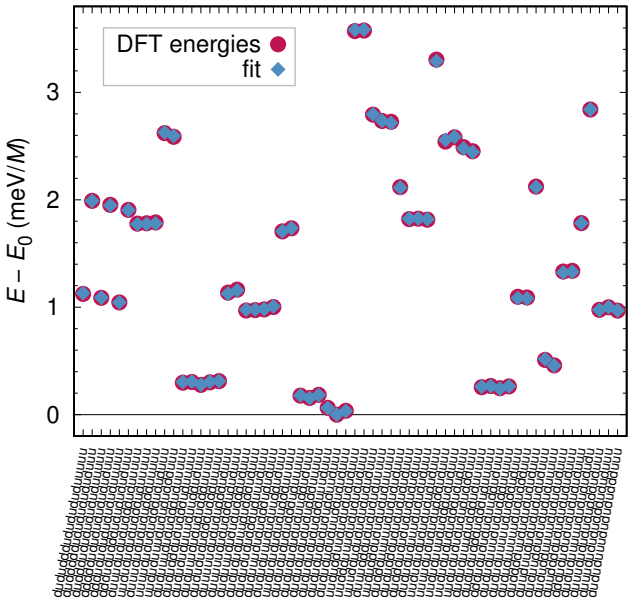

Figure S5. DFT energies for 60 spin configurations in a 5-fold unit cell of $CuAg(SO_4)_2$ at $U_{\rm Ag} = 3.6\,$eV, $U_{\rm Cu} = 4.8\,$eV, compared to the energies of the Heisenberg Hamiltonian with the fitted parameters given in the first line of Table S1. The fit is excellent.

Details of the classical Monte Carlo method

In the classical Monte Carlo (CMC) calculations, we perform the standard single spin-flip technique with Metropolis updates. We apply as many Metropolis updates as there are spins in the unit cell in each Monte Carlo step. For thermalization, we use 100,000 Monte

$M1\,M2$	U_{Ag}	U_{Cu}	J_1	J_2^{A}	J_2^{C}	J_3	J_4	J_5^{A}	J_5^{C}	θ_{CW}
$d_{M1\,M2}$ (Å)			AgCu	AgAg	CuCu	AgCu	AgCu	AgAg	CuCu	
			3.579	4.734		4.961	5.727	6.017		
	3.6	4.8	-3.6(1.2)	3.2(1.6)	35.2(9)	5.6(4)	169.5(4)	93.4(6)	-0.6(5)	-142
	3.65	**4.87**	**-3.4(1.2)**	**3.0(1.6)**	**34.4(9)**	**5.4(4)**	**168.6(4)**	**91.9(6)**	**-0.5(5)**	**-140**
	4.2	5.6	-1.5(9)	1.6(1.2)	26.7(6)	4.2(3)	150.3(3)	79.0(5)	-0.4(3)	-123
	4.8	6.4	-0.2(6)	0.6(9)	20.1(5)	3.4(2)	134.2(2)	68.5(4)	-0.3(3)	-108
	5.4	7.2	0.4(5)	0.1(7)	14.9(4)	2.8(2)	120.2(2)	61.0(3)	-0.2(2)	-96

$M1\,M2$	U_{Ag}	U_{Cu}	J_6	J_7^{A}	J_7^{C}	J_8^{A}	J_8^{C}	J_{10}	J_{13}	J_{16}^{A}	J_{16}^{C}	θ_{CW}
$d_{M1\,M2}$ (Å)			AgCu	AgAg	CuCu	AgAg	CuCu	AgCu	AgCu	AgAg	CuCu	
			6.134	6.215		7.158		8.332	8.846	9.266		
	3.6	4.8	-2.6(7)	-0.4(7)	-3.9(5)	-2.2(3.6)	0.5(1.2)	0.5(4)	0.4(2)	1.0(4)	0.0(3)	-142
	3.65	**4.87**	**-2.5(7)**	**-0.4(7)**	**-3.8(5)**	**-2.1(3.6)**	**0.5(1.2)**	**0.5(4)**	**0.3(2)**	**0.9(4)**	**0.0(3)**	**-140**
	4.2	5.6	-2.0(5)	-0.4(5)	-2.7(3)	-1.6(2.6)	0.3(9)	0.4(3)	0.2(2)	0.7(3)	0.0(2)	-123
	4.8	6.4	-1.6(4)	-0.4(4)	-2.0(3)	-1.2(1.9)	0.2(6)	0.3(2)	0.2(1)	0.5(2)	0.0(2)	-108
	5.4	7.2	-1.2(3)	-0.3(3)	-1.5(2)	-0.9(1.4)	0.2(5)	0.2(2)	0.1(1)	0.4(2)	0.0(1)	-96

Table S1. All calculated exchange parameters for $CuAg(SO_4)_2$. The line in bold face is interpolated by demanding that the set of couplings yield the experimentally observed Curie-Weiss temperature of $\theta_{\mathrm{CW}} = -140\,\mathrm{K}$ [2].

Carlo steps. After thermalization, we use 10,000 Monte Carlo steps to measure physical quantities A. A averages are calculated from spin configurations at intervals of 10 Monte Carlo steps. In this study, A are total energy E, magnetization M and spin structure factor

$$S(\mathbf{q}) = \sum_{ij} \mathbf{S}_i \cdot \mathbf{S}_j e^{i\mathbf{q}\cdot(\mathbf{r}_i - \mathbf{r}_j)} \tag{S7}$$

where $\mathbf{r}_i$ is the position of spin i. At the end of measurements, we calculate averages $\langle A \rangle_{\mathrm{MC}}$ of the measured physical quantities and calculate specific heat

$$C = k_{\mathrm{B}} \frac{\langle E^2 \rangle_{\mathrm{MC}} - \langle E \rangle_{\mathrm{MC}}^2}{T^2} \tag{S8}$$

and susceptibility

$$\chi = \frac{1}{N} \frac{\langle \mathbf{M}^2 \rangle_{\mathrm{MC}} - \langle |\mathbf{M}| \rangle_{\mathrm{MC}}^2}{k_{\mathrm{B}} T} \tag{S9}$$

where k_{B} is the Boltzmann constant, T is temperature, N is the number of spins in the unit cell, $\mathbf{M}$ is magnetization, and E is total energy. We repeat this set of thermalization and measurements 160 times and calculate average and standard deviations of C, χ and $\langle S(\mathbf{q}) \rangle_{\mathrm{MC}}$ for all sets.

Magnetooptics

In order to estimate the size of the altermagnetic effect in this compound we have calculated, using the built-in capability in the VASP code[5–8] (using *Ag_pv, Cu_pv, S* and *O* projector augmented wave potentials, energy cutoff of 400 eV, 500 valence bands, and a k-mesh of $9\times6\times9$) the full matrix dielectric function, assuming the Neél vector as suggested by the calculations, perpendicular to the ab plane, and found a sizeable antisymmetric contribution in the xz channel (note that symmetry also allows a nondiagonal *symmetric* ϵ_{xz}). The results are shown in Fig. S6.

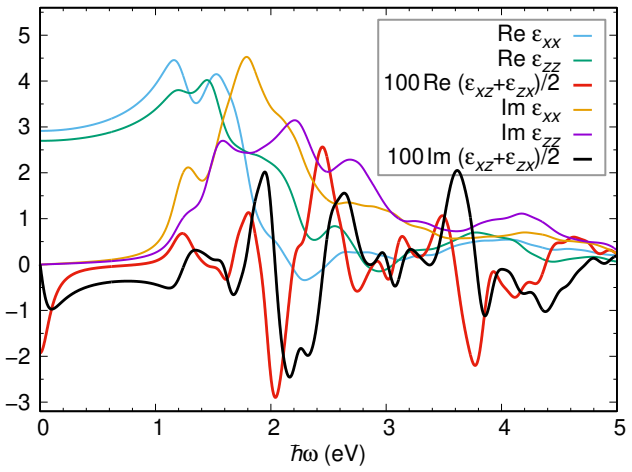

Figure S6. Calculated diagonal and asymmetric off-diagonal dielectric function. The latter is on the order of 1% of the former, which is considered sizeable in magnetooptics.

Relativistic effects

We use fully relativistic GGA and GGA+U calculation in order to check for effects of spin-orbit coupling. Analyzing the total energies of the ground state AFM order in the unit cell of $CuAg(SO_4)_2$, we find some anisotropy. At the GGA level, choosing x, y and z as magnetic quantization axis, we find moments to be easy axis along z with y direction 0.09 meV/f.u. higher and x 0.15 meV/f.u. higher in energy. At the relevant U value for $CuAg(SO_4)_2$, $U_{\mathrm{Ag}} = 3.6\,\mathrm{eV}$, $U_{\mathrm{Cu}} = 4.8\,\mathrm{eV}$, x becomes easy axis with y direction 0.24 meV/f.u. higher

and z 1.4 meV/f.u. higher in energy.

[1] H. Kim, K. Shiozaki, and S. Murakami, Glide-symmetric magnetic topological crystalline insulators with inversion symmetry, Phys. Rev. B **100**, 165202 (2019).

[2] M. Domański, Z. Mazej, and W. Grochala, A unique two-dimensional silver(II) antiferromagnet $Cu[Ag(SO_4)_2]$ and perspectives for its further modifications, Chem. Eur. J. **29**, e202302042 (2023).

[3] H. O. Jeschke, F. Salvat-Pujol, E. Gati, N. H. Hoang, B. Wolf, M. Lang, J. A. Schlueter, and R. Valentí, Barlowite as a canted antiferromagnet: Theory and experiment, Phys. Rev. B **92**, 094417 (2015).

[4] K. Iida, H. K. Yoshida, A. Nakao, H. O. Jeschke, Y. Iqbal, K. Nakajima, S. Ohira-Kawamura, K. Munakata, Y. Inamura, N. Murai, M. Ishikado, R. Kumai, T. Okada, M. Oda, K. Kakurai, and M. Matsuda, $q = 0$ long-range magnetic order in centennialite $CaCu_3(OD)_6Cl_2 \cdot {}_0 \cdot 6\,D_2O$: A spin-$\frac{1}{2}$ perfect kagome antiferromagnet with J_1-J_2-J_d, Phys. Rev. B **101**, 220408 (2020).

[5] G. Kresse and J. Hafner, Ab initio molecular dynamics for liquid metals, Phys. Rev. B **47**, 558 (1993).

[6] G. Kresse and J. Furthmüller, Efficiency of ab-initio total energy calculations for metals and semiconductors using a plane-wave basis set, Comput. Mater. Sci. **6**, 15 (1996).

[7] G. Kresse and J. Furthmüller, Efficient iterative schemes for ab initio total-energy calculations using a plane-wave basis set, Phys. Rev. B **54**, 11169 (1996).

[8] G. Kresse and D. Joubert, From ultrasoft pseudopotentials to the projector augmented-wave method, Phys. Rev. B **59**, 1758 (1999).